metals

MDPI

Article

Efficient Synthesis of Alkali Borohydrides from Mechanochemical Reduction of Borates Using Magnesium–Aluminum-Based Waste

Thi Thu Le [1], Claudio Pistidda [1,*], Julián Puszkiel [1,2], Chiara Milanese [3], Sebastiano Garroni [4], Thomas Emmler [1], Giovanni Capurso [1], Gökhan Gizer [1], Thomas Klassen [1,5] and Martin Dornheim [1]

1 Institute of Materials Research, Materials Technology, Helmholtz-Zentrum Geesthacht GmbH, Max-Planck-Strasse 1, Geesthacht D-21502, Schleswig-Holstein, Germany; thi.le@hzg.de (T.T.L.); julianpuszkiel1979@gmail.com (J.P.); thomas.emmler@hzg.de (T.E.); giovanni.capurso@hzg.de (G.C.); goekhan.gizer@hzg.de (G.G.); thomas.klassen@hzg.de (T.K.); martin.dornheim@hzg.de (M.D.)

2 Department of Physical chemistry of Materials, Consejo Nacional de Investigaciones Científicas y Técnicas (CONICET) and Centro Atómico Bariloche, Av. Bustillo km 9500 S.C. de Beriloche, Argentina

3 Pavia H2 Lab, C.S.G.I. & Department of Chemistry, Physical Chemistry Section, University of Pavia, 27100 Pavia, Italy; chiara.milanese@unipv.it

4 Department of Chemistry and Pharmacy and INSTM, University of Sassari, Via Vienna 2, 07100 Sassari, Italy; sgarroni@uniss.it

5 Helmut Schmidt University, University of the Federal Armed Forces Hamburg, D-22043 Hamburg, Germany

* Correspondence: claudio.pistidda@hzg.de; Tel.: +49-4152-87-2644

Received: 23 August 2019; Accepted: 24 September 2019; Published: 29 September 2019

Abstract: Lithium borohydride ($LiBH_4$) and sodium borohydride ($NaBH_4$) were synthesized via mechanical milling of $LiBO_2$, and $NaBO_2$ with Mg–Al-based waste under controlled gaseous atmosphere conditions. Following this approach, the results herein presented indicate that $LiBH_4$ and $NaBH_4$ can be formed with a high conversion yield starting from the anhydrous borates under 70 bar H_2. Interestingly, $NaBH_4$ can also be obtained with a high conversion yield by milling $NaBO_2{\cdot}4H_2O$ and Mg–Al-based waste under an argon atmosphere. Under optimized molar ratios of the starting materials and milling parameters, $NaBH_4$ and $LiBH_4$ were obtained with conversion ratios higher than 99.5%. Based on the collected experimental results, the influence of the milling energy and the correlation with the final yields were also discussed.

Keywords: alkali borohydrides; Mg–Al waste; ball milling; high conversion yield

1. Introduction

Tetrahydroborates, discovered in the 1940s, have been attracting the attention of the scientific community in the last decades as possible energy vectors. Although tetrahydroborates, such as $LiBH_4$ and $NaBH_4$, are commonly used as reducing agents in organic and inorganic chemistry [1–4], their employment as potential hydrogen storage materials have also been investigated, due to their high gravimetric hydrogen densities. $LiBH_4$ and $NaBH_4$ feature very attractive gravimetric and volumetric hydrogen storage capacities, i.e., of 18.5 wt.% H_2 and 10.8 wt.% H_2, and 113.1 kg H_2/m^3 and 121 kg H_2/m^3, respectively [2–4]. In particular, their use as single hydrides [5–12] and their combination in the so-called reactive hydride composites (RHCs) approach were intensively studied [13–28]. These tetrahydroborates were first synthesized by Schlesinger and Brown by reacting diborane with ethyl lithium to form $LiBH_4$ [29] and with sodium trimethoxyborohydride to form $NaBH_4$ [30]. Since then, several studies attempted to improve the synthesis of these two tetrahydroborates [31–39]. Nowadays,

$LiBH_4$ is produced in several ways, i.e., $LiBH_4$ is mechanically prepared via the reaction of $NaBH_4$ and LiBr using ball milling (Reaction (1)) or via the reaction of BF_3 and LiH under diethyl ether (Reaction (2)). $LiBH_4$ can be also synthesized through a costly process from individual elements (Li, B) under high hydrogen pressure (up to 1000 bar, Reaction (3)), or after an extensive reactive milling process from LiH and B under milder pressure conditions. For commercial purposes, $NaBH_4$ is produced through the Brown–Schlesinger process treating NaH with methyl borate–$B(OCH_3)_3$ at 225 to 275 °C (Reaction (4)) [40]. The drawbacks associated with the use of this method are the utilization of expensive reducing agents on the one side, and the necessity to carry it out through a multiple-step process on the other side; all of which significantly affects the cost of the final product. Due to the kinetic constraints evidenced by the boron metal, the reactive milling of sodium hydride with the respective metal boride, MgB_2, has represented a valid strategy, despite the final yield not overcoming 15 wt. % of borohydride [41]. A second method used industrially for the production of $NaBH_4$ is referred to as the Bayer process [42,43]. In this process, $Na_2B_4O_7$, Na, and SiO_2 are heated up to 700 °C under hydrogen atmosphere (Reaction (5)). Due to the low melting point of sodium (97.8 °C), it seems that Reaction (5) takes place partially in a molten state. It must be noticed that, due to the high temperature and hydrogen pressure, this process exhibits potential explosion risks. In addition, the disposal of Na_2SiO_3 is a further issue to be considered when using this process to produce $NaBH_4$.

$$NaBH_4 + LiBr \rightarrow NaBr + LiBH_4, \quad (1)$$

$$BF_3 + 4\ LiH \rightarrow LiBH_4 + 3\ LiF, \quad (2)$$

$$Li + B + 2H_2 \rightarrow LiBH_4, \quad (3)$$

$$B(OCH_3)_3 + 4\ NaH \rightarrow NaBH_4 + 3\ NaOCH_3, \quad (4)$$

$$Na_2B_4O_7 + 16\ Na + 8\ H_2 + 7\ SiO_2 \rightarrow 4\ NaBH_4 + 7\ Na_2SiO_3. \quad (5)$$

In the literature, several works on the conversion of borates of Na and Li using high-purity MgH_2 are reported. Li et al. [32] investigated the possibility of synthesizing $NaBH_4$ by ball milling-dehydrated $Na_2B_4O_7$ with MgH_2 in the presence of Na-based compounds (e.g., NaOH, Na_2CO_3, and Na_2O_2). Kojima and Haga. [34] published that a reaction yield equal to 98 % of $NaBH_4$ can be obtained when annealing a mixture of $NaBO_2$ with Mg_2Si under 7 MPa of hydrogen pressure at 550 °C for 2 to 4 h. Kong et al. [33], Hsueh et al. [36] and Çakanyıldırım et al. [44] independently investigated the possibility of forming $NaBH_4$ from a mixture of MgH_2 and $NaBO_2$ ball milled in argon atmosphere. In their works, Kong et al., Hsueh et al., and Çakanyıldırım et al. achieved an $NaBH_4$ yield of above 70%. Similarly, Bilen et al. [37] achieved 90% $LiBH_4$ purity from the reaction of $LiBO_2$ with MgH_2 by ball milling. In addition, ball milling is known to be an extremely powerful and versatile technique for the treatment of waste materials [45–49]. These works clearly show that ball milling is a suitable method to produce $LiBH_4$ and $NaBH_4$ from mixtures of $LiBO_2$ or $NaBO_2$ and MgH_2, respectively. However, in view of possible large-scale production of these borohydrides, due to the production costs associated with the use of high-purity MgH_2, the above-mentioned processes are not economically feasible. In order to tackle the production cost issue, the possibility of replacing MgH_2 with cost-neutral wastes, such as Mg–Al-based alloys, was pursued in this work. The prepared samples were characterized by XRD, FT-IR, and MAS-NMR techniques. The results of this investigation are presented and thoroughly discussed in the following sections.

2. Materials and Methods

Lithium metaborate ($LiBO_2$, anhydrous ≥ 98% purity, Sigma Aldrich) and sodium metaborate tetrahydrate ($NaBO_2{\cdot}4H_2O$, 99% purity, Sigma Aldrich) were purchased in powder form. As suggested by the differential thermal analysis (DTA) shown in Figure S1, $NaBO_2$ was obtained by heating

$NaBO_2{\cdot}4H_2O$ up to 350 °C. The waste Mg–Al-based alloys used in this work were obtained from the in-house technical workshop at the Helmholtz-Zentrum Geesthacht in the form of swarf/chips of a few millimeter sizes (Figure S2). These scrap particles were kept in air before the beginning of the experimental activity. The composition determined via spark emission spectrum analysis is: 76.09 wt.% Mg, 13.6 wt.% Al, 0.06 wt.% Ca, 0.13 wt.% Cu, 0.13 wt.% Mn, 0.45 wt.% Nd, 8.6 wt.% Zn, 0.24 wt.% Y, 0.7 wt.% Ag. All the specimens were prepared and handled in a glove box under continuously purified argon atmosphere (<10 ppm O_2 and H_2O) to avoid any further oxidation of the starting materials.

In order to reduce the particles' size, the as-received waste material was milled in argon atmosphere for 2 h using a Simoloyer CM08 mill (Zoz GmbH, Wenden, Germany) in a batch of 350 g with 5 mm 100Cr6 steel balls using a ball to powder ratio (BPR) of 20:1. The material morphology was characterized by scanning electron microscopy (EvoMA10, Zeiss, Oberkochen, Germany) at the University of Pavia (Italy). In order to avoid moisture and/or oxygen contaminations during the sample preparation, a small amount of material was placed on a special Al sample holder inside a dedicated argon filled glove box (<1 ppm O_2 and H_2O). The sample holder was then evacuated before transporting it to the SEM and was opened only after a high vacuum had been created inside the SEM chamber.

The mechanochemical reaction was conducted by ball milling a mixture of Mg–Al waste and dehydrated borates under high hydrogen pressure in a planetary mill. Since Mg accounts for 76.09 wt.% in the Mg–Al-based waste, mixtures of anhydrous $LiBO_2$ or $NaBO_2$ and Mg–Al-based waste (as designated in Table 1) were prepared with respect to the amount of Mg contained in the Mg-Al-based waste; that is, the molar ratio of borate and Mg was 1:2. For example, in this experimental study, for the synthesis of the LBOM batch, the amount of $LiBO_2$ and Mg–Al waste was fixed at 2.430 and 3.121 g, respectively. Similarly, the calculated amount $NaBO_2$ and Mg–Al waste was 2.697 and 2.779 g, respectively, for NBOM synthesis. The reaction components were put into a high-pressure vial (from Evico magnetics GmbH, Dresden, Germany). The milling process was performed under 70 bar of hydrogen with a BPR of 20:1, using a speed of 500 rpm and milling times in the range between 1 and 36 h. An attempt to synthesize $NaBH_4$ directly from $NaBO_2{\cdot}4H_2O$ and Mg–Al-based waste was made by milling the mixture under 1 bar of argon pressure for 36 h (i.e., the amount of $NaBO_2.4H_2O$ and Mg–Al waste was fixed at 2.448 and 3.558 g, respectively). For the sake of simplicity, the description and designation of the mixtures prepared and investigated in this work are reported as in Table 1.

Table 1. Designation of the investigated materials.

No	Material	Designation
1	$LiBO_2$ + Mg–Al-based waste	LBOM
2	$NaBO_2$ + Mg–Al-based waste	NBOM
3	$NaBO_2{\cdot}4H_2O$ + Mg–Al-based waste	NBOM·H_2O

The hours of milling that the system underwent are indicated by the number following the sample name (e.g., NBOM_36 is the system $NaBO_2$ + Mg–Al-based waste milled for 36 h).

In order to evaluate the studied process from the thermodynamic point of view, equilibrium composition calculations were performed with the HSC Chemistry software 9.7 [50]. The calculations were done based on the thermodynamic data available for the phases involved in the syntheses. For these calculations, a hydrogen pressure of 70 bar, a vial volume of 200 cm^3, and a temperature between 25 and 40 °C were considered (Table 2). Since Mg accounted for 76.09 wt.% in the Mg–Al-based waste, stoichiometric ratios were used with respect to the amount of Mg contained in the Mg–Al-based waste as indicated in Table 2.

Table 2. Stoichiometric compositions with respect to the amount of Mg in Mg–Al-based waste of starting materials, milling atmosphere, and proposed products.

System	Stoichiometric Mixture of Starting Materials	Milling Temperature	Vial Volume	H_2 Pressure
1	$LiBO_2$(s) + 2Mg(s) + 2H_2(g) (Total amount of Mg–Al-based waste: 2.5 mol)	25–40 °C	200 cm^3	70 bar
2	$NaBO_2$(s) + 2Mg(s) + 2H_2(g) (Total amount of Mg–Al-based waste: 2.5 mol)	25–40 °C	200 cm^3	70 bar
3	$NaBO_2$·4H_2O(s) + 6Mg(s) (Total amount of Mg–Al-based waste: 7.25 mol)	25–40 °C	200 cm^3	70 bar

X-ray diffraction (XRD) analyses were carried out using a Bruker D8 Discover diffractometer (Bruker AXS GmbH, Karlsruhe, Germany) equipped with a Cu Kα radiation (λ = 1.54184 Å) X-ray source and a VÅNTEC-500 area detector. The diffraction patterns were acquired in nine steps in the 2θ range from 10° to 90°, with an exposure time of 300 s per step and a step size of 10°. A small amount of powder was placed onto a sample holder and sealed with an airtight dome made of polymethylmethacrylate (PMMA), which is transparent to X-rays.

The composition of the synthesized samples was also characterized by means of the FT-IR technique (Cary 630 FTIR spectrometer, Agilent Technologies Deutschland GmbH, Waldbronn, Germany). For each measurement, the background was calibrated, a small amount of material was placed on the diamond ATR top plate, and the FT-IR spectrum was acquired in the frequency range 4000–400 cm^{-1}, with a spectral resolution of 4 cm^{-1}.

The composition of both the starting material containing boron and the milling products was also investigated by means of ^{11}B Solid State MAS-NMR using a 500-MHz (^{11}B frequency: 160.46 MHz) Bruker Avance III HD NMR spectrometer (Bruker BioSpin GmbH, Rheinstetten, Germany) equipped with a Bruker 4 mm BB/1H-19F probe. Rotation speeds in the range of 8 to 12 kHz were applied. To overcome the broad ^{11}B background of the standard bore probe, the vendor-supplied "zgbs" sequence was employed. The repetition time of the experiments was chosen in such a way that the sample was fully relaxed.

Energy Transfer during the Milling

Ball milling (BM) is a well-recognized technique to promote physical and chemical transformations into solid and liquid systems [51–53]. Among all top-down approaches, BM can be considered as one of today's most used techniques for the production of hydrogen storage materials by using different apparatuses, namely, the attritor mill, vibration mill, and planetary mill. Basically, BM consists of repeated collision events, which involve solid materials trapped between the balls and reactor vial walls. The microscopic transformations are accompanied by macroscopic evidences, which can be estimated by characterization techniques, such as powder XRD. The handling of the milling parameters and the mechanisms behind the process can lead to improvements in the performance in the synthesis of new materials. In this context, the estimation of the mechanical energy transferred to the powders during milling represents one of the most important parameters for monitoring the efficiency of the milling and defining the reproducibility of the synthesis.

The energy, P^*, from the mill transferred to the powders per mass unit during the milling process in a planetary ball mill was then estimated using the model proposed by Burgio et al. [54], based on Equation (1):

$$P^* = -\varphi_b \cdot N_b \cdot m_b \cdot t \cdot \left(\Omega_p - \omega_v\right) \cdot \left[\frac{\omega_v^3 \cdot \left(r_v - \frac{d_b}{2}\right)}{\Omega_p} + \Omega_p \cdot \omega_v \cdot R_p\right] \cdot \frac{\left(r_v - \frac{d_b}{2}\right)}{2 \cdot \pi \cdot m_p}, \quad (1)$$

where φ is the degree of milling, N_b is the number of balls, m_b is the mass of balls (kg), t is the milling time (s), Ω_p is the rotation speed of the plate (rad/s), ω_v is the rotation velocity of vial (rad/s), r_v is the vial radius (m), R_p is the plate radius (m), d_b is the ball diameter (m), and m_p is the mass of the material (kg). The results of this calculation correlated to the results of the experimental techniques allow the energy

that is transferred to the system in order to reach the maximum yield to be obtained. The influence of every different process parameter on the energy transferred during the milling processes was also recently studied in a methodical analysis based on Equation (1) for hydrogen storage materials [55].

3. Results and Discussions

The morphology of the Mg–Al-based waste after milling was characterized by means of the SEM technique (Figure 1). Compared to the starting material (ESI, Figure S2), the shape and size of the milled product were considerably changed. The ribbon-like structure of several hundred micrometers, which characterized the material received from the workshop, is not visible any longer; in its place, slightly elongated particles, with an average size between 10 and 70 μm, are observed. More details about the evolution of this waste alloy as a hydrogen storage material can be found in the literature [46].

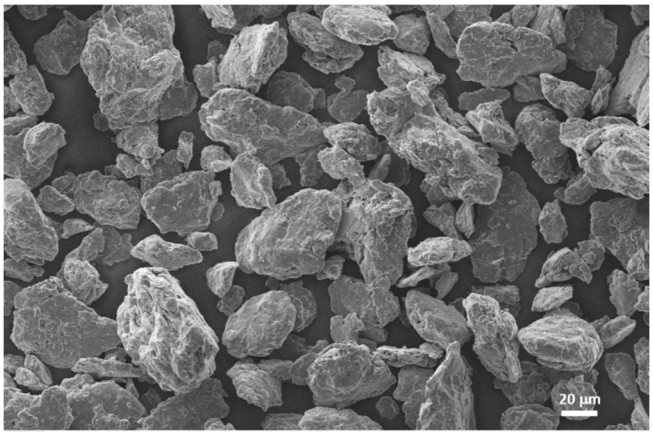

Figure 1. SEM image of the as-milled Mg–Al-based waste.

The equilibrium composition calculations (refer to SI Figures S3–S6 and Tables S1–S6) performed for the stoichiometric mixtures $LiBO_2$ + 2Mg and $NaBO_2$ + 2Mg (total amount of Mg–Al-based waste: 2.5 mol) under 70 bar H_2, and $NaBO_2{\cdot}4H_2O$ + 6Mg (total amount of Mg–Al-based waste: 7.25 mol) under 1 bar Ar, show that the calculated values for the Gibbs free energy (ΔG°) associated to Reactions (6) to (8) are largely negative, in agreement with a previously published work [56]. The mechanochemical synthesis then leads to the formation of the respective borohydrides and MgO (s).

$$LiBO_2(s) + 2Mg(s) + 2H_2(g) \rightarrow LiBH_4(s) + 2MgO(s)\ \Delta G^\circ = -299.7\ kJ, \quad (6)$$

$$NaBO_2(s) + 2Mg(s) + 2H_2(g) \rightarrow NaBH_4(s) + 2MgO(s)\ \Delta G^\circ = -343.2\ kJ, \quad (7)$$

$$NaBO_2{\cdot}4H_2O(s) + 6Mg(s) \rightarrow NaBH_4(s) + 6MgO(s) + 2H_2(g)\ \Delta G^\circ = -1651\ kJ. \quad (8)$$

It is noteworthy that the formation of borohydrides did not occur (Reaction (9)) when ball milling a mixture of Al and borates under the same hydrogen pressure and milling conditions applied in the previous synthesis:

$$4Al + 3NaBO_2 + 6H_2 \rightarrow 3NaBH_4 + 2Al_2O_3. \quad (9)$$

Given the fact that the use of a 1:2 metaborate:magnesium stoichiometric ratio only leads to the formation of the respective borohydride plus MgO, this ratio was used for the experimental investigations. After 36 h of mechanical treatment in hydrogen atmosphere, the samples were characterized via the SEM technique and the results are displayed in Figure 2. The system NBOM_36 (Figure 2a) appears to be constituted of particles, which occasionally agglomerate in a wide size range, whereas the sample LBOM_36 (Figure 2b) seems to form some flakes. In both cases, the particle sizes of the powders after milling are much finer in comparison to the starting materials.

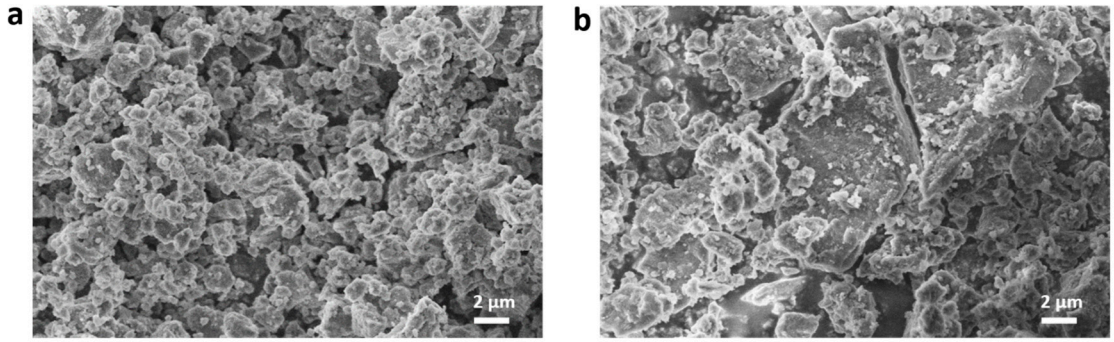

Figure 2. SEM images of the samples (**a**) NBOM_36 and (**b**) LBOM_36.

Figure 3 shows the XRD patterns acquired for the systems NBOM and LBOM for different milling times (Figure 3a,b, respectively). For comparison, the diffraction patterns of the starting materials, as well as those of the expected borohydrides, are also shown. In the diffraction patterns of NBOM_1, it is clearly possible to see the reflections of magnesium, in addition to the weak diffraction peaks attributed to the presence of $NaBO_2$. After 12 h of milling (NBOM_12), the diffraction peaks of MgO are detected. In the diffraction patterns acquired after 24 h of milling (NBOM_24), the peaks of MgO are clearly visible. In addition, small peaks belonging to a yet unknown phase (2θ = 28.39°, 32.04°, 38.33°, and 47.24°) are also present. Interestingly, in the diffraction patterns of NBOM_36, the diffraction peaks of $NaBH_4$ are observed together with those of MgO. In the diffraction patterns of LBOM_1, the diffraction peaks of the starting materials (Mg and $LiBO_2$) are still visible. The patterns of LBOM_12, LBOM_24, and LBOM_36 (Figure 3B(e)–(g)) are characterized by the presence of the diffraction peaks of MgO only. For these systems, even after 36 h of milling, it is not possible to observe the formation of crystalline $LiBH_4$ by XRD.

The specimens were characterized by the FT-IR technique to detect the possible presence of non-crystalline species. Figure 4, and Tables 3 and 4 show the infrared vibration bands observed in the starting and ball-milled materials. The vibrational spectra of borates are constantly complicated due to the capability of coordinating the three and four oxygen atoms of boron atoms to formulate either a monomer or a polymer form. The IR spectrum of the $NaBO_2$ sample was characterized as shown in Figure 4A(a). The band, which appeared at around 1225 cm^{-1}, can be assigned to the B-O stretching vibrations of BO_4 units. Another band at 1395 cm^{-1} is attributed to the asymmetric stretching of the B-O bond of trigonal BO_3. These values were similarly found in [57,58]. For pure $NaBH_4$ (Figure 4A(b)), the measured absorption band for the B-H bending mode is 1108 cm^{-1}, whereas the bands of the B-H stretching mode are found at 2208 and 2278 cm^{-1}. In the FT-IR spectrum acquired for the sample NBOM_1, only the absorption bands of $NaBO_2$ are visible. The spectra of the samples NBOM_12, NBOM_24, and NBOM_36 show the characteristic absorption bands of B-H bending modes at 1118 and 1113 cm^{-1}, respectively, whereas the absorption bands of B-H stretching modes are observed at 2286, 2294, and 2288 cm^{-1}, respectively. The $NaBH_4$ stretching band at 2214 cm^{-1} is only observed in the spectrum of NBOM_36. All the $NaBH_4$ FT-IR absorption bands in the ball-milled NBOM are slightly shifted to a higher frequency compared to the values of pure $NaBH_4$. This effect eventually originates from the presence of other compounds intimately mixed with $NaBH_4$. Similarly to $NaBO_2$, the IR spectrum of $LiBO_2$ was recorded as in Figure 4B(a): In this case, two distinguished bands emerge due to the B-O stretching vibrations of the BO_4 groups (1140 cm^{-1}) and of the trigonal BO_3 groups (1420 cm^{-1}). In Figure 4B(b), the B-H bending bands measured for pure $LiBH_4$ are found at 1089 and 1232 cm^{-1}, whereas the stretching bands are observed at 2270 and 2298 cm^{-1}. Those results are in accordance with a previous report [59]. The spectrum of LBOM_1 does not show features associated with the presence of $LiBH_4$. However, the spectra of the material milled for 12, 24, and 36 h (LBOM_12, LBOM_24, and LBOM_36, respectively) clearly show the characteristic bending and stretching absorption bands of $LiBH_4$ at about 1090 and 2300 cm^{-1}, respectively. In addition to the absorption bands at 1091 and

2301 cm^{-1}, in the spectrum of LBOM_36, bands at 1232 and 2272 cm^{-1} are also visible. This finding indicates that the amount of $LiBH_4$ present in the sample increases between 24 and 36 h of milling.

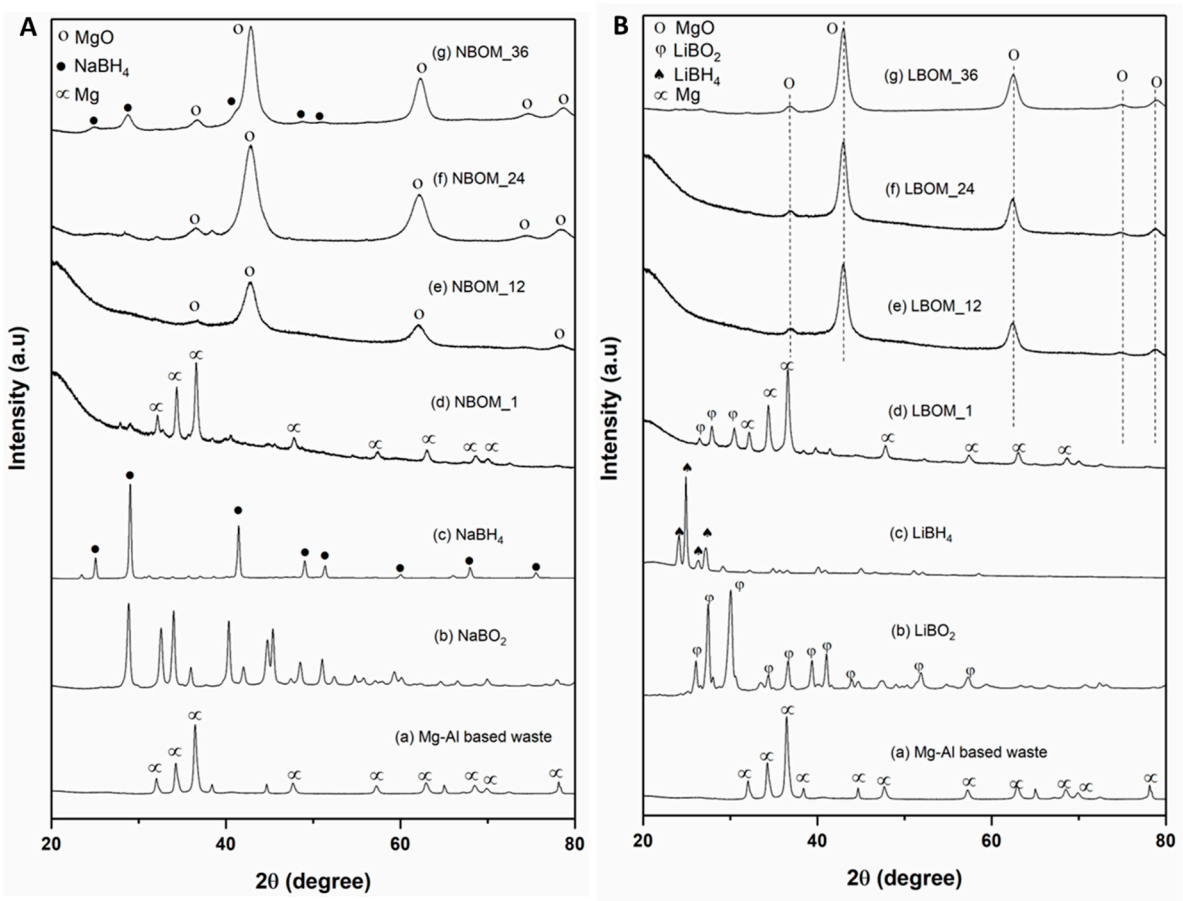

Figure 3. XRD patterns of materials (**A**): (a) Mg–Al-based alloy; (b) $NaBO_2$; (c) $NaBH_4$; (d) NBOM_1; (e) NBOM_12; (f) NBOM_24, and (g) NBOM_36; (**B**): (a) Mg-based alloy; (b) $LiBO_2$; (c) $LiBH_4$; (d) LBOM_1; (e) LBOM_12; (f) LBOM_24, and (g) LBOM_36.

Table 3. Infrared vibration bands of $NaBH_4$, $NaBO_2$, and ball-milled materials at different milling time durations at room temperature.

Frequencies (cm^{-1})	$NaBH_4$	$NaBO_2$	NBOM_1	NBOM_12	NBOM_24	NBOM_36
B-H Bending Modes	1108	-	-	1118	1118	1113
	-	-	-	-	-	-
B-H Stretching Modes	2208	1225	-	-	-	2214
	2278	1423	-	2286	2294	2288

Table 4. Infrared vibration bands of $LiBH_4$, $LiBO_2$, and ball-milled materials at different milling time durations at room temperature.

Frequencies (cm^{-1})	$LiBH_4$	$LiBO_2$	LBOM_1	LBOM_12	LBOM_24	LBOM_36
B-H Bending Modes	1089	-	-	1093	1092	1091
	1232	-	-	-	-	1232
B-H Stretching Modes	2270	1140	-	-	-	2272
	2298	1420	-	2311	2301	2302

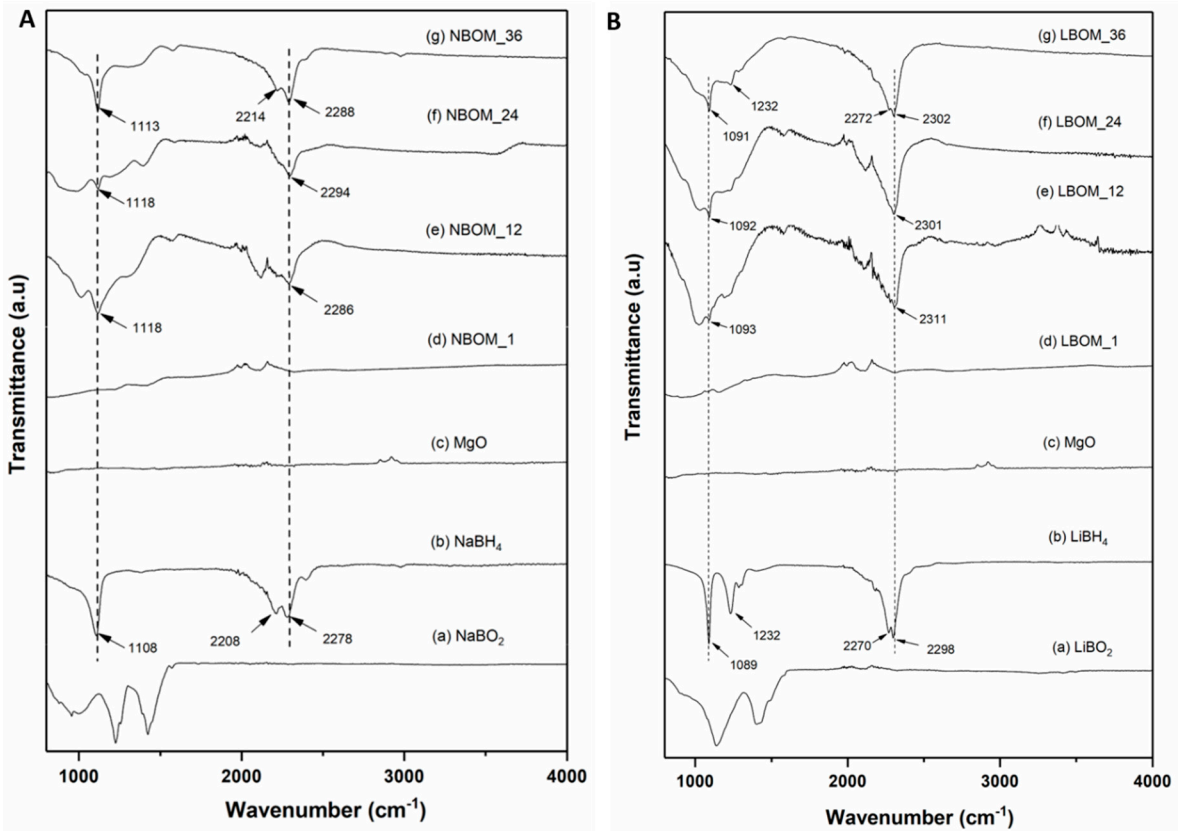

Figure 4. FT-IR spectra of materials: (**A**) (a) $NaBO_2$.; (b) $NaBH_4$; (c) MgO; (d) NBOM_1; (e) NBOM_12; (f) NBOM_24; and (g) NBOM_36; (**B**) (a) $LiBO_2$; (b) $LiBH_4$; (c) MgO; (d) LBOM_1; (e) LBOM_12; (f) LBOM_24; and (g) LBOM_36.

To better understand the nature of the obtained products and to quantify the reaction yields, the samples were also investigated via ^{11}B MAS-NMR. Figure 5 shows the acquired ^{11}B MAS-NMR spectra for the reference and ball-milled materials. In Figure 5A, the NMR spectra of pure $NaBH_4$ and $NaBO_2$ and those of the milled NBOM system are shown. The spectra of all the NBOM specimens (Figure 5A(d)–(f)) are dominated by the resonance of $NaBH_4$ at −42.2 ppm. Additionally, the resonance of small quantities of boron oxide around 1 ppm are visible (SI, Figure S9). Upon integration of the spectra, boron oxide accounts for the 2.8%, 1.8%, and 0.3%, of the spectra-integrated intensity of NBOM_12, NBOM_24, and NBOM_36, respectively. The determination of the $NaBH_4$ yield followed the procedure described in reference [32]. The conversion ratio of $NaBO_2$ into $NaBH_4$, which was calculated based on the integration of the MAS-NMR signals, is approximately 97.2%, 98.2%, and 99.7% for NBOM_12, NBOM_24, and NBOM_36, respectively. No formation of $NaBH_4$ was observed for NBOM_1, in agreement with the XRD and FT-IR results. Similarly, in the ^{11}B MAS-NMR spectrum of LBOM specimens (Figure 5B (c)–(f)), the sharp resonance of $LiBH_4$ is observed at –41.4 ppm. The analysis of the signals of the MAS-NMR spectra shows that boron oxide contributes to 1.6%, 1.1%, and 0.4% of the total ^{11}B MAS-NMR-integrated intensity for LBOM_12, LBOM_24, and LBOM_36, respectively. This implies that the conversion yield of $LiBO_2$ into $LiBH_4$ is approximately 98.4%, 98.9%, and 99.6% for LBOM_12, LBOM_24, and LBOM_36, respectively. The ^{11}B MAS-NMR spectrum of LBOM_1 does not show the presence of $LiBH_4$.

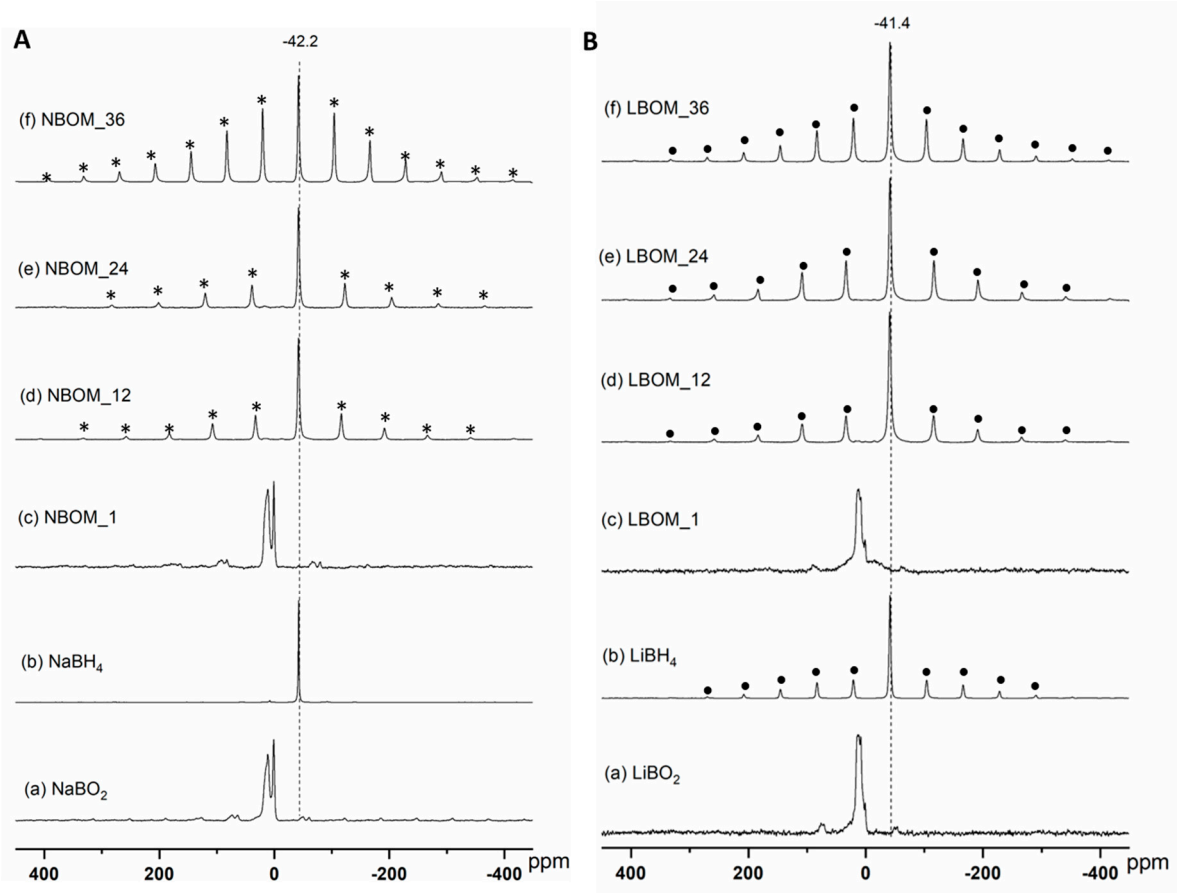

Figure 5. ^{11}B MAS-NMR spectra of materials: (**A**) (a) $NaBO_2$, (b) $NaBH_4$, (c) NBOM_1, (d) NBOM_12, (e) NBOM_24 and (f) NBOM_36; (**B**) (a) $LiBO_2$, (b) $LiBH_4$, (c) LBOM_1, (d) LBOM_12, (e) LBOM_24, and (f) LBOM_36. Spinning sideband resonances from $NaBH_4$ and $LiBH_4$ are indicated by asterisks (*) and solid circles (●), respectively.

Although the use of ball mills for carrying out mechanochemical driven processes is often advantageous from the point of view of the time necessary to complete the process and from the perspective of its scalability, the need to apply high gas pressure within the drum of the mill is a technical challenge that is difficult to overcome. Recently, Felderhoff et al. [60] reported the possibility of partially reversing the hydrolysis of $NaBH_4$ by ball milling from the hydrolysis by-product $NaBO_2{\cdot}2H_2O$ with high-purity Mg in an argon atmosphere. As a result of their investigation, they achieved a maximum conversion yield of 68.55%.

Inspired by this work, an attempt was made to synthesize $NaBH_4$ starting from a mixture of $NaBO_2{\cdot}4H_2O$ and Mg–Al-based waste. The molar ratio between metaborate and Mg contained in the waste was 1:6, as shown in Table 2. The milling process was carried out in Ar atmosphere instead of H_2 gas. Figure 6 shows the XRD diffraction patterns and FT-IR spectra of the reference materials and of the ball-milled material. In Figure 6A(d), for the sample NBOM·H_2O_36, besides the diffraction peaks of MgO, in agreement with the diffraction patterns of pure $NaBH_4$ (Figure 6A(c)), the reflections belonging to $NaBH_4$ at $2\theta = 25.15°$, 29.01°, and 41.45° are visible. In Figure 6B, the FT-IR spectra of $NaBO_2{\cdot}4H_2O$, $NaBH_4$, MgO, and NBOM·H_2O_36 are shown. The FT-IR spectrum of NBOM·H_2O_36 (Figure 6B(d)), similarly to that of pure $NaBH_4$, shows absorption bands of the bending mode of $NaBH_4$ at 1114 cm^{-1} and of the stretching modes at 2225 and 2289 cm^{-1}. Therefore, the presence of $NaBH_4$ was confirmed by both XRD and FT-IR techniques.

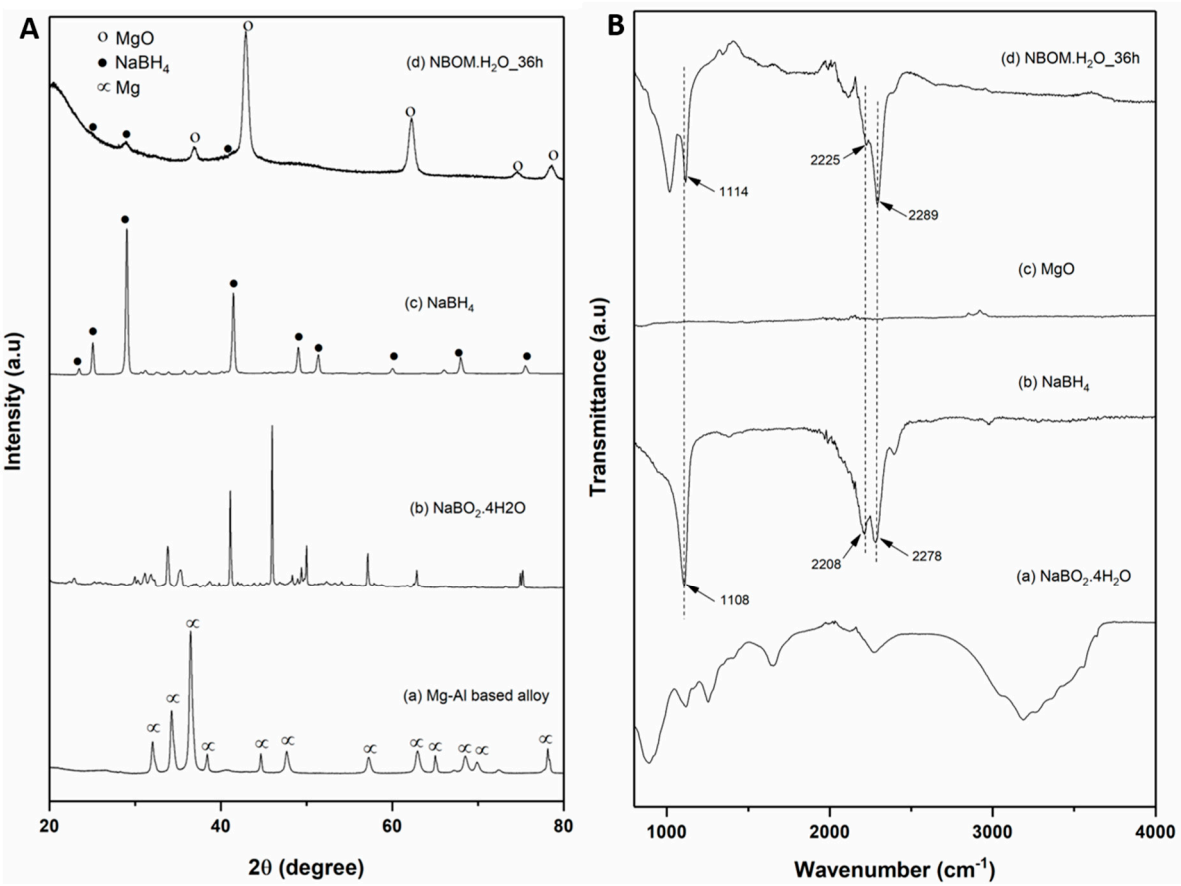

Figure 6. (**A**) XRD diffractions of: (a) Mg–Al-based alloy, (b) $NaBO_2 \cdot 4H_2O$, (c) $NaBH_4$, (d) ball-milled $NBOM \cdot H_2O$ at 36 h under 1 bar Ar, (**B**) FT-IR spectra of materials: (a) $NaBO_2 \cdot 4H_2O$; (b) $NaBH_4$; (c) MgO and ball-milled $NBOM \cdot H_2O$ at 36 h under 1 bar Ar.

Figure 7 shows the ^{11}B MAS-NMR spectra of pure $NaBH_4$ and $NBOM \cdot H_2O\_36$. The $NaBH_4$ resonance of pure $NaBH_4$ (Figure 7a) at −42.2 ppm is also observed for the sample $NBOM \cdot H_2O\_36$ (Figure 7b). Less intense signals around 1 ppm, belonging to boron oxide, are also observed. Based on the integrated signals of the $NaBH_4$ and boron oxide, it is possible to claim that the conversion ratio of $NaBO_2 \cdot 4H_2O$ to $NaBH_4$ is >99.5%.

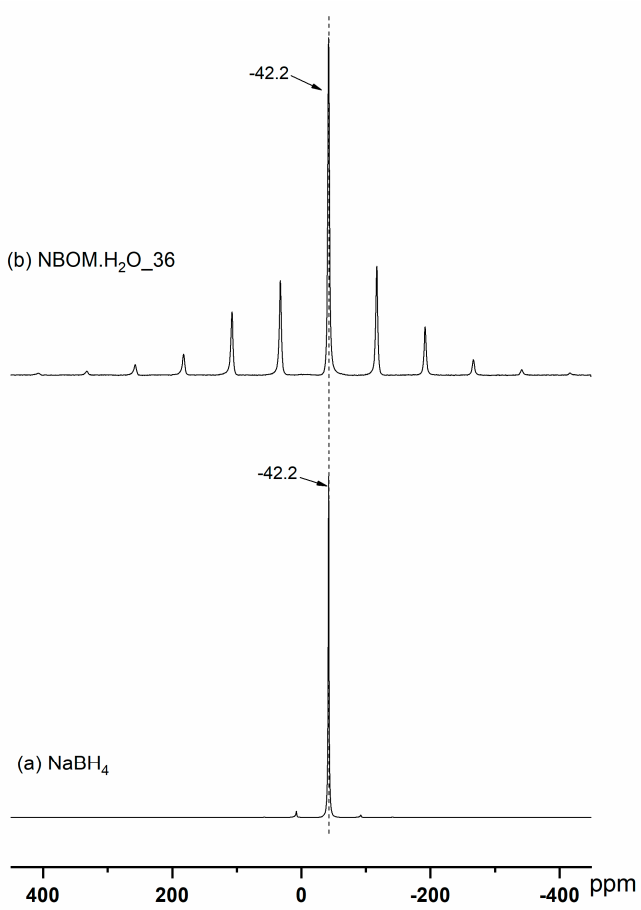

Figure 7. NMR spectra of $NaBH_4$ and NBOM·H_2O milled for 36 h under 1 bar Ar.

The synthesized borohydrides ($LiBH_4$ and $NaBH_4$) can be completely separated from the by-products (mainly MgO) by an extraction process with isopropylamine and ethylenediamine (EDA) followed by a purification process [36,37], as described in SI. This further step is the object of ongoing research.

The model developed by Burgio et al. was used (Equation (1)) to quantify the energy required for the almost full conversion of the starting materials into borohydrides and to assure the reproducibility of the production processes, mainly at the time used when scaling up the reaction. These calculations were performed for the first two systems (refer to Table 1) as evidence that the milling process can be completely characterized to avoid the cost and time required by a trial-and-error procedure with large amounts of materials. Figure 8 presents the correlation between the milling time, the total transferred energy, and the conversion ratio for NBOM and LBOM materials. All parameters, including the BPR, velocity, and mass of powders, were the same for all the samples, thus the energy dissipated at each impact was the same for the entire milling time (SI, Table S7). The milling energy per gram of powder changes with the milling time varying from 1 to 36 h. According to Equation (1), the transferred energy depends on the filling vial coefficient, which is related to the number of balls and reactor volume, as well as to the volume of powder [54]. In this study, the number of balls and reactor volume were the same for all experiments; therefore, the energy transferred was mainly related to the volume occupied by each powder sample [55]. Taking into account that the densities of the initial reagents were not so different, the energy transferred for NBOM and LBOM materials was almost the same (Figure 8). The experimental results (XRD and FT-IR) show that increasing milling time leads to higher yields of borohydrides. Therefore, according to the above-described calculations, 228 Wh/g corresponding to 36 h of milling process is required for $NaBH_4$ and $LiBH_4$ conversion ratios over 99.7% and 99.6%, respectively.

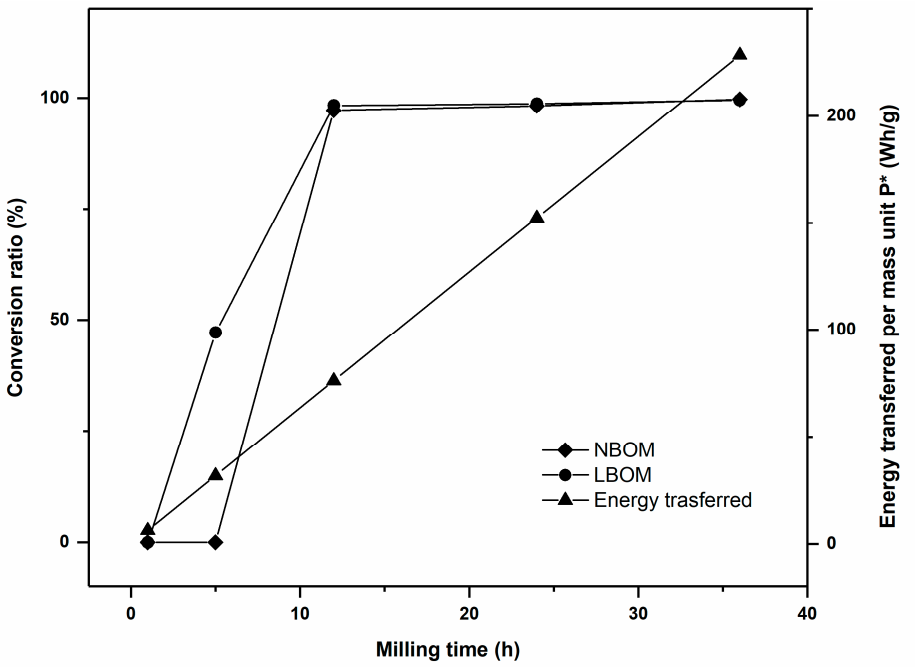

Figure 8. Correlation between conversion and milling energy as a function of the milling time.

According to the results shown in Figure 8, it would also be possible to reduce the milling time to 12 h with the same conversion ratio. In this experimental study, however, the test was prolonged to 36 h to assess the effects of the milling time on the powder morphology, pureness, and nanostructure. A lower energy consumption, without compromising the yield, is nevertheless fundamental in order to estimate the parameters for scaling up the process. According to Equation (1), it is theoretically possible to increase the mass of the powder milled if all the other factors are increased accordingly, to transfer the same amount of energy in the process.

In practice, however, the size of synthesis is limited by the milling apparatus available. The problem of industrial production of hydride materials has already been considered [61]. The limit to the use of larger industrial devices (where geometries and sizes are larger, masses and forces are higher, but the nature of the process is the same [62]) are controlled by the atmosphere. Non-reactive materials can easily be considered for processing in industrial machines, but when an inert or a reactive atmosphere is required, the batch size is limited by the possibility of properly sealing the milling environment in such dynamic apparatuses [53,63]. Recently, more sophisticated milling processes were developed using larger machines (up to a 100-L milling volume), where the vial is static and the atmosphere is monitored [64]. This would allow for semi-industrial synthesis of borohydrides from a mechanochemical reduction of borates, as well.

The kinetics of $LiBH_4$ formation, determined by quantitative analysis of its solid-state NMR patterns, was obtained by plotting the $LiBH_4$ fraction, α, as a function of the milling time (Figure 9). The kinetic curve has a sigmoidal shape that is well represented by the empirical Equation (2) [65]:

$$\alpha = 1 - (1 + kt)\exp(-kt), \quad (2)$$

where α represents the mass fraction of $LiBH_4$ formed during the mechanochemical reaction and k is the apparent rate constant. The best-fitted line (dark full line) allows an estimate of the k value for the $LiBH_4$ formation process, which is equal to 5.68 10^{-3} min^{-1}, one order of magnitude higher, for example, than the one estimated in the mechanically-induced metathesis reaction of $Mg(NH_2)_2$ (8.39 10^{-4} min^{-1}) [66]. In contrast, $NaBH_4$ was not identified for the sample after 5 h of ball milling. There might be an induction period for the $NaBH_4$ conversion under the given conditions. It is claimed that

a different mechanism seems to occur in $NaBH_4$ formation during BM, with respect to those shown by $LiBH_4$. For this reason, further experiments are now in progress to clarify this interesting point.

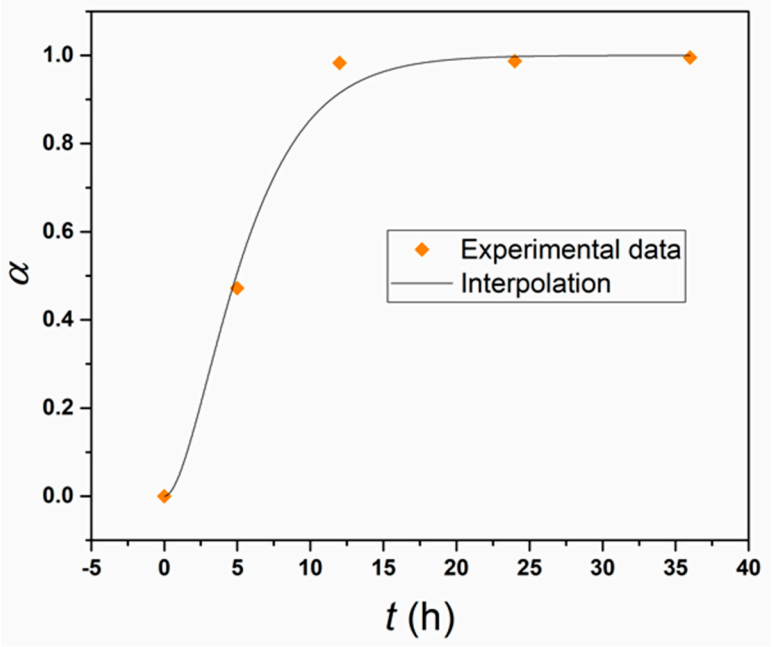

Figure 9. Fraction of $LiBH_4$ phase obtained by milling $LiBO_2$ plus Mg-Al-based waste, as a function of time (h).

4. Conclusions

This work demonstrated that the synthesis of $NaBH_4$ and $LiBH_4$ from low-cost starting materials, such as metaborate compounds and Mg-Al waste, employing a common industrial method, such as ball milling, is efficiently possible. The mechanochemical synthesis allows for the use of different conditions, such as hydrogen and argon atmosphere under room temperature, both leading to high yields of conversions in the case of $NaBH_4$. The advantage of using $NaBO_2{\cdot}4H_2O$ as a starting material, without any need for water elimination, improves the efficiency of the synthesis method. Experimental results (XRD, FT-IR and NMR results) confirmed that $NaBH_4$ and $LiBH_4$ were successfully synthesized under 70 bar H_2 and room temperature by ball milling, achieving conversion efficiencies of $NaBH_4$ and $LiBH_4$ over 99.5%. It is interesting to emphasize that $NaBH_4$ can be directly produced from $NaBO_2{\cdot}4H_2O$ plus Mg-Al-based waste under 1 bar Ar and room temperature by ball milling, and the conversion ratio of $NaBO_2$ to $NaBH_4$ can be as high as 99.5%.

Supplementary Materials: The following are available online at http://www.mdpi.com/2075-4701/9/10/1061/s1. Figure S1: DTA of $NaBO_2{\cdot}4H_2O$ measured at argon atmosphere from RT to 380 °C with a heating rate of 5 °C/min, Figure S2: The Mg-Al based waste as received from the workshop, Figure S3. ΔG vs. T, Figure S4. ΔG vs. T. Figure S5. ΔG vs. T. Figure S6. ΔG vs. T, Figure S7. ΔG vs. T, Figure S8. ΔG vs. T, Figure S9. An inset of NMR spectra in range of 10 ppm to −10 ppm, Figure S10. Schematic diagram of a Soxhlet extractor, Figure S11. Schematic diagram of a hydrogen evolution apparatus. Table S1: Calculated amounts (mol%) of equilibrium species. Conditions: 25–40 °C and 70 bar H2 and 25–40 °C and 1 bar H2. The amount of H2(s) is not take into account in the calculated amounts, Table S2. Reaction under 70 bar H2 condition, Table S3. Calculated amounts (mol %) of equilibrium species. Conditions: 25–40 °C and 70 bar H2. The amount of H2 (s) is not take into account in the calculated amounts, Table S4. Reaction under 70 bar H2 condition, Table S5. Calculated amounts (mol %) of equilibrium species. Conditions: 25–40 °C and 1 bar Ar, Table S6. Reaction under the milling conditions, Table S7. Energy transferred to powder during milling.

Author Contributions: Conceptualization, T.T.L., C.P. and G.G.; formal analysis, T.T.L. and G.G.; investigation, T.T.L.; resources, J.P., C.M., S.G., T.E. and G.C.; supervision, C.P.; writing–original draft, T.T.L.; writing–review & editing, C.P., T.K. and M.D.

Funding: This research was funded by the European Marie Curie ITN Action–ECOSTORE project, grant number 607040. The authors also thank CONICET (Consejo Nacional de Invetigaciones Científicas y Técnicas) and Alexander von Humboldt Foundation (Fellowship number: ARG–1187279–GF-P).

Conflicts of Interest: The authors declare no conflict of interest. The funders had no role in the design of the study; in the collection, analyses, or interpretation of data; in the writing of the manuscript, or in the decision to publish the results.

References

1. Yamamoto, J. *Sodium Borohydride Digest*; Rohm, H., Ed.; Industrial Chemicals and Additives: Danvers, MA, USA, 2003.
2. Paskevicius, M.; Jepsen, L.H.; Schouwink, P.; Cerny, R.; Ravnsbaek, D.B.; Filinchuk, Y.; Dornheim, M.; Besenbacher, F.; Jensen, T.R. Metal borohydrides and derivatives-synthesis, structure and properties. *Chem. Soc. Rev.* **2017**, *46*, 1565–1634. [CrossRef] [PubMed]
3. Puszkiel, J.; Garroni, S.; Milanese, C.; Gennari, F.; Klassen, T.; Dornheim, M.; Pistidda, C. Tetrahydroborates: Development and Potential as Hydrogen Storage Medium. *Inorganics* **2017**, *5*, 74. [CrossRef]
4. Züttel, A.; Wenger, P.; Rentsch, S.; Sudan, P.; Mauron, P.; Emmenegger, C. LiBH4 a new hydrogen storage material. *J. Power Sources* **2003**, *118*, 1–7. [CrossRef]
5. Loghmani, M.H.; Shojaei, A.F. Synthesis and characterization of Co–La–Zr–B quaternary amorphous nano alloy: Kinetic study for hydrogen generation from hydrolysis of sodium borohydride. *J. Alloy. Compd.* **2013**, *580*, 61–66. [CrossRef]
6. Ai, L.; Liu, X.; Jiang, J. Synthesis of loofah sponge carbon supported bimetallic silver–cobalt nanoparticles with enhanced catalytic activity towards hydrogen generation from sodium borohydride hydrolysis. *J. Alloy. Compd.* **2015**, *625*, 164–170. [CrossRef]
7. Bandal, H.A.; Jadhav, A.R.; Kim, H. Cobalt impregnated magnetite-multiwalled carbon nanotube nanocomposite as magnetically separable efficient catalyst for hydrogen generation by NaBH4 hydrolysis. *J. Alloy. Compd.* **2017**, *699*, 1057–1067. [CrossRef]
8. Chen, W.; Ouyang, L.Z.; Liu, J.W.; Yao, X.D.; Wang, H.; Liu, Z.W.; Zhu, M. Hydrolysis and regeneration of sodium borohydride (NaBH4)—A combination of hydrogen production and storage. *J. Power Sources* **2017**, *359*, 400–407. [CrossRef]
9. Wang, M.C.; Ouyang, L.Z.; Liu, J.W.; Wang, H.; Zhu, M. Hydrogen generation from sodium borohydride hydrolysis accelerated by zinc chloride without catalyst: A kinetic study. *J. Alloy. Compd.* **2017**, *717*, 48–54. [CrossRef]
10. Liu, H.; Jiao, L.; Zhao, Y.; Cao, K.; Liu, Y.; Wang, Y.; Yuan, H. Improved dehydrogenation performance of LiBH4 by confinement into porous TiO2 micro-tubes. *J. Mater. Chem. A* **2014**, *2*, 9244–9250. [CrossRef]
11. Zhao, Y.; Liu, Y.; Liu, H.; Kang, H.; Cao, K.; Wang, Q.; Zhang, C.; Wang, Y.; Yuan, H.; Jiao, L. Improved dehydrogenation performance of LiBH4 by 3D hierarchical flower-like MoS2 spheres additives. *J. Power Sources* **2015**, *300*, 358–364. [CrossRef]
12. Orimo, S.; Nakamori, Y.; Kitahara, G.; Miwa, K.; Ohba, N.; Towata, S.; Züttel, A. Dehydriding and rehydriding reactions of LiBH4. *J. Alloy. Compd.* **2005**, *404–406*, 427–430. [CrossRef]
13. Bösenberg, U.; Doppiu, S.; Mosegaard, L.; Barkhordarian, G.; Eigen, N.; Borgschulte, A.; Jensen, T.R.; Cerenius, Y.; Gutfleisch, O.; Klassen, T.; et al. Hydrogen sorption properties of MgH2–LiBH4 composites. *Acta Mater.* **2007**, *55*, 3951–3958. [CrossRef]
14. Bösenberg, U.; Kim, J.W.; Gosslar, D.; Eigen, N.; Jensen, T.R.; von Colbe, J.M.B.; Zhou, Y.; Dahms, M.; Kim, D.H.; Günther, R. Role of additives in LiBH4–MgH2 reactive hydride composites for sorption kinetics. *Acta Mater.* **2010**, *58*, 3381–3389. [CrossRef]
15. Bösenberg, U.; Ravnsbaek, D.B.; Hagemann, H.; D'Anna, V.; Bonatto Minella, C.; Pistidda, C.; Beek, W.V.; Jensen, T.R.; Bormann, R.; Dornheim, M. Pressure and Temperature Influence on the Desorption Pathway of the LiBH4-MgH2. *J. Phys. Chem. C* **2010**, *114*, 15212–15217. [CrossRef]
16. Bosenberg, U.; Vainio, U.; Pranzas, P.K.; von Colbe, J.M.; Goerigk, G.; Welter, E.; Dornheim, M.; Schreyer, A.; Bormann, R. On the chemical state and distribution of Zr- and V-based additives in reactive hydride composites. *Nanotechnology* **2009**, *20*, 204003. [CrossRef] [PubMed]

17. Deprez, E.; Justo, A.; Rojas, T.C.; López-Cartés, C.; Bonatto Minella, C.; Bösenberg, U.; Dornheim, M.; Bormann, R.; Fernández, A. Microstructural study of the LiBH4–MgH2 reactive hydride composite with and without Ti-isopropoxide additive. *Acta Mater.* **2010**, *58*, 5683–5694. [CrossRef]
18. Deprez, E.; Muñoz-Márquez, M.A.; Roldañ, M.A.; Prestipino, C.; Palomares, F.J.; Minella, C.B.; Bösenberg, U.; Dornheim, M.; Bormann, R.; Fernández, A. Oxidation State and Local Structure of Ti-Based Additives in the Reactive Hydride Composite 2LiBH4+ MgH2. *J. Phys. Chem. C* **2010**, *114*, 3309–3317. [CrossRef]
19. Fan, M.; Sun, L.; Zhang, Y.; Xu, F.; Zhang, J.; Chu, H. The catalytic effect of additive Nb2O5 on the reversible hydrogen storage performances of LiBH4–MgH2 composite. *Int. J. Hydrog. Energy* **2008**, *33*, 74–80. [CrossRef]
20. Li, Y.; Izuhara, T.; Takeshita, H.T. Promotional Effect of Aluminum on MgH_2+$LiBH_4$ Hydrogen Storage Materials. *Mater. Trans.* **2011**, *52*, 641–646. [CrossRef]
21. Liu, B.H.; Zhang, B.J.; Jiang, Y. Hydrogen storage performance of LiBH4+1/2MgH_2 composites improved by Ce-based additives. *Int. J. Hydrog. Energy* **2011**, *36*, 5418–5424. [CrossRef]
22. Pinkerton, F.E.; Meyer, M.S.; Meisner, G.P.; Balogh, M.P.; Vajo, J.J. Phase Boundaries and Reversibility of $LiBH_4$/MgH_2 Hydrogen Storage Material. *J. Phys. Chem. C* **2007**, *111*, 12881–12885. [CrossRef]
23. Puszkiel, J.A.; Gennari, F.C.; Larochette, P.A.; Ramallo-López, J.M.; Vainio, U.; Karimi, F.; Pranzas, P.K.; Troiani, H.; Pistidda, C.; Jepsen, J.; et al. Effect of Fe additive on the hydrogenation-dehydrogenation properties of 2LiH + MgB_2/2$LiBH_4$ + MgH_2 system. *J. Power Sources* **2015**, *284*, 606–616. [CrossRef]
24. Sridechprasat, P.; Suttisawat, Y.; Rangsunvigit, P.; Kitiyanan, B.; Kulprathipanja, S. Catalyzed $LiBH_4$ and MgH_2 mixture for hydrogen storage. *Int. J. Hydrog. Energy* **2011**, *36*, 1200–1205. [CrossRef]
25. Vajo, J.J.; Skeith, S.L. Reversible Storage of Hydrogen in Destabilized $LiBH_4$. *Phys. Chem. B Lett.* **2005**, *109*, 3719–3722. [CrossRef] [PubMed]
26. Wang, P.; Ma, L.; Fang, Z.; Kang, X.; Wang, P. Improved hydrogen storage property of Li–Mg–B–H system by milling with titanium trifluoride. *Energy Environ. Sci.* **2009**, *2*, 120–123. [CrossRef]
27. Puszkiel, J.; Castro Riglos, M.V.; Karimi, F.; Santoru, A.; Pistidda, C.; Klassen, T.; Bellosta von Colbe, J.M.; Dornheim, M. Changing the Dehydrogenation Pathway of $LiBH_4$–MgH_2 via Nanosized Lithiated TiO2. *Phys. Chem. Chem. Phys.* **2017**, *19*, 7455–7460. [CrossRef] [PubMed]
28. Pistidda, C.; Garroni, S.; Bonatto Minella, C.; Dolci, F.; Jensen, T.R.; Nolis, P.; Bösenberg, U.; Cerenius, Y.; Lohstroh, W.; Fichtner, M.; et al. Pressure Effect on the 2NaH + MgB_2 Hydrogen Absorption Reaction. *J. Phys. Chem. C* **2010**, *114*, 21816–21823. [CrossRef]
29. Schlesinger, H.I.; Sanderson, R.T.; Burg, A.B. Metallo Borohydrides. I. Aluminum Borohydride. *J. Am. Chem. Soc.* **1940**, *62*, 3421–3425. [CrossRef]
30. Schlesinger, H.I.; Brown, H.C.; Hoekstra, H.R.; Rapp, L.R. Reactions of Diborane with Alkali Metal Hydrides and Their Addition Compounds. New Syntheses of Borohydrides. Sodium and Potassium Borohydrides1. *J. Am. Chem. Soc.* **1953**, *75*, 199–204. [CrossRef]
31. Liu, B.H.; Li, Z.P.; Zhu, J.K. Sodium borohydride formation when Mg reacts with hydrous sodium borates under hydrogen. *J. Alloy. Compd.* **2009**, *476*, L16–L20. [CrossRef]
32. Li, Z.P.; Morigazaki, N.; Liu, B.H.; Suda, S. Preparation of sodium borohydride by the reaction of MgH2 with dehydrated borax through ball milling at room temperature. *J. Alloy. Compd.* **2003**, *349*, 232–236. [CrossRef]
33. Kong, L.; Cui, X.; Jin, H.; Wu, J.; Du, H.; Xiong, T. Mechanochemical Synthesis of Sodium Borohydride by Recycling Sodium Metaborate. *Energy Fuels* **2009**, *23*, 5049–5054. [CrossRef]
34. Kojima, Y.; Haga, T. Recycling Process of Sodium Metaborate to Sodium Borohydride. *Int. J. Hydrog. Energy* **2003**, *28*, 989–993. [CrossRef]
35. Kantürk Figen, A.; Pişkin, S. Microwave assisted green chemistry approach of sodium metaborate dihydrate (NaBO2·2H2O) synthesis and use as raw material for sodium borohydride (NaBH4) thermochemical production. *Int. J. Hydrog. Energy* **2013**, *38*, 3702–3709. [CrossRef]
36. Hsueh, C.-L.; Liu, C.-H.; Chen, B.-H.; Chen, C.-Y.; Kuo, Y.-C.; Hwang, K.-J.; Ku, J.-R. Regeneration of spent-NaBH4 back to NaBH4 by using high-energy ball milling. *Int. J. Hydrog. Energy* **2009**, *34*, 1717–1725. [CrossRef]
37. Bilen, M.; Yılmaz, O.; Gürü, M. Synthesis of LiBH4 from LiBO2 as hydrogen carrier and its catalytic dehydrogenation. *Int. J. Hydrog. Energy* **2015**, *40*, 15213–15217. [CrossRef]
38. Atiyeh, H.K.; Davis, B.R. Separation of sodium metaborate from sodium borohydride using nanofiltration membranes for hydrogen storage application. *Int. J. Hydrog. Energy* **2007**, *32*, 229–236. [CrossRef]

39. Agresti, F.; Khandelwal, A. Evidence of formation of $LiBH_4$ by high-energy ball milling of LiH and B in a hydrogen atmosphere. *Scr. Mater.* **2009**, *60*, 753–755. [CrossRef]
40. Schlesinger, H.I.; Brown, H.C.; Finholt, A.E. The Preparation of Sodium Borohydride by the High Temperature Reaction of Sodium Hydride with Borate Esters. *J. Am. Chem. Soc.* **1953**, *75*, 205–209. [CrossRef]
41. Garroni, S.; Minella, C.B.; Pottmaier, D.; Pistidda, C.; Milanese, C.; Marini, A.; Enzo, S.; Mulas, G.; Dornheim, M.; Baricco, M.; et al. Mechanochemical synthesis of NaBH4 starting from NaH–MgB_2 reactive hydride composite system. *Int. J. Hydrog. Energy* **2013**, *38*, 2363–2369. [CrossRef]
42. Broja, G.; Schlabacher, W. Process for the Production of Alkali Metal Borohydrides. DE Patent 1,108,670, 6 October 1959.
43. Schubert, F.; Lang, K.; Schlabacher, W. Process for the Production of Borohydrides. DE Patent 1,067,005, 1959.
44. Çakanyıldırım, Ç.; Gürü, M. Processing of $NaBH_4$ from $NaBO_2$ with MgH_2 by ball milling and usage as hydrogen carrier. *Renew. Energy* **2010**, *35*, 1895–1899. [CrossRef]
45. Pistidda, C.; Bergemann, N.; Wurr, J.; Rzeszutek, A.; Møller, K.T.; Hansen, B.R.S.; Garroni, S.; Horstmann, C.; Milanese, C.; Girella, A.; et al. Hydrogen storage systems from waste Mg alloys. *J. Power Sources* **2014**, *270*, 554–563. [CrossRef]
46. Hardian, R.; Pistidda, C.; Chaudhary, A.L.; Capurso, G.; Gizer, G.; Cao, H.; Milanese, C.; Girella, A.; Santoru, A.; Yigit, D.; et al. Waste Mg-Al based alloys for hydrogen storage. *Int. J. Hydrog. Energy* **2018**, *43*, 16738–16748. [CrossRef]
47. Baláž, M. Ball milling of eggshell waste as a green and sustainable approach: A review. *Adv. Colloid Interface Sci.* **2018**, *256*, 256–275. [CrossRef] [PubMed]
48. Ou, Z.; Li, J.; Wang, Z. Application of mechanochemistry to metal recovery from second-hand resources: A technical overview. *Environ. Sci. Process. Impacts* **2015**, *17*, 1522–1530. [CrossRef] [PubMed]
49. Guo, X.; Xiang, D.; Duan, G.; Mou, P. A review of mechanochemistry applications in waste management. *Waste Manag.* **2010**, *30*, 4–10. [CrossRef] [PubMed]
50. *Outokumpu HSC Chemistry for Windows*, version 9.7; Outokumpu Research Oy: Pori, Finland, 2009.
51. Baláž, P.; Achimovičová, M.; Baláž, M.; Billik, P.; Cherkezova-Zheleva, Z.; Criado, J.M.; Delogu, F.; Dutková, E.; Gaffet, E.; Gotor, F.J.; et al. Hallmarks of mechanochemistry: From nanoparticles to technology. *Chem. Soc. Rev.* **2013**, *42*, 7571–7637. [CrossRef]
52. Humphry-Baker, S.A.; Garroni, S.; Delogu, F.; Schuh, C.A. Melt-driven mechanochemical phase transformations in moderately exothermic powder mixtures. *Nat. Mater.* **2016**, *15*, 1280. [CrossRef] [PubMed]
53. Suryanarayana, C. Mechanical alloying and milling. *Prog. Mater. Sci.* **2001**, *46*, 1–184. [CrossRef]
54. Burgio, N.; Iasonna, A.; Magini, M.; Martelli, S.; Padella, F. Mechanical alloying of the Fe−Zr system. Correlation between input energy and end products. *IL Nuovo Cimento D* **1991**, *13*, 459–476. [CrossRef]
55. Jepsen, J.; Capurso, G.; Puszkiel, J.; Busch, N.; Werner, T.; Milanese, C.; Girella, A.; Bellosta von Colbe, J.; Dornheim, M.; Klassen, T. Effect of the Process Parameters on the Energy Transfer during the Synthesis of the 2LiBH4-MgH2 Reactive Hydride Composite for Hydrogen Storage. *Metals* **2019**, *9*, 349. [CrossRef]
56. Dean, J.A. *Lange's Handbook of Chemistry*; McGraw-Hill: New York, NY, USA, 1999.
57. Erfani, M.; Saion, E.; Soltani, N.; Hashim, M.; Wan Abdullah, W.S.B.; Navasery, M. Facile Synthesis of Calcium Borate Nanoparticles and the Annealing Effect on Their Structure and Size. *Int. J. Mol. Sci.* **2012**, *13*, 14434–14445. [CrossRef] [PubMed]
58. Kaur, M.; Singh, S.P.; Mudahar, D.S.; Mudahar, G.S. Structural Investigation Of B_2O_3-Li_2CO_3-Al_2O_3 Glasses By Molar Volume Measurements And Ftir Spectroscopy. *Mater. Phys. Mech.* **2012**, *15*, 66–73.
59. D'Anna, V.; Spyratou, A.; Sharma, M.; Hagemann, H. FT-IR spectra of inorganic borohydrides. *Spectrochim. Acta Part A Mol. Biomol. Spectrosc.* **2014**, *128*, 902–906. [CrossRef] [PubMed]
60. Ouyang, L.; Chen, W.; Liu, J.; Felderhoff, M.; Wang, H.; Zhu, M. Enhancing the Regeneration Process of Consumed $NaBH_4$ for Hydrogen Storage. *Adv. Energy Mater.* **2017**, *7*, 1700299. [CrossRef]
61. Eigen, N.; Keller, C.; Dornheim, M.; Klassen, T.; Bormann, R. Industrial production of light metal hydrides for hydrogen storage. *Scr. Mater.* **2007**, *56*, 847–851. [CrossRef]
62. Gock, E.; Kurrer, K.-E. Eccentric vibratory mills–Theory and practice. *Powder Technol.* **1999**, *105*, 302–310. [CrossRef]
63. Burmeister, C.F.; Kwade, A. Process engineering with planetary ball mills. *Chem. Soc. Rev.* **2013**, *42*, 7660–7667. [CrossRef] [PubMed]

64. Bellosta von Colbe, J.M.; Puszkiel, J.; Capurso, G.; Franz, A.; Benz, H.U.; Zoz, H.; Klassen, T.; Dornheim, M. Scale-up of milling in a 100 L device for processing of TiFeMn alloy for hydrogen storage applications: Procedure and characterization. *Int. J. Hydrog. Energy* **2019**. [CrossRef]
65. Delogu, F.; Takacs, L. Information on the mechanism of mechanochemical reaction from detailed studies of the reaction kinetics. *J. Mater. Sci.* **2018**, *53*, 13331–13342. [CrossRef]
66. Garroni, S.; Delogu, F.; Bonatto Minella, C.; Pistidda, C.; Cuesta-Lopez, S. Mechanically activated metathesis reaction in $NaNH_2$–MgH_2 powder mixtures. *J. Mater. Sci.* **2017**, *52*, 11891–11899. [CrossRef]